

Sorption and desorption properties of a $\text{CaH}_2/\text{MgB}_2/\text{CaF}_2$ Reactive Hydride Composite as potential hydrogen storage material

K. Suarez Alcantara¹, U. Boesenberg¹, O. Zavorotynska², J. Bellosta von Colbe¹, K. Taube¹, M. Baricco², T. Klassen¹, M. Dornheim¹

¹ Institute of Materials Research, Materials Technology, Helmholtz-Zentrum Geesthacht, D-21502 Geesthacht Germany

² Università di Torino, NIS Centre of Excellence, Dipartimento di Chimica I.F.M. Via P.Giuria 7. I-10125 Torino, Italy.

Abstract

The hydrogenation behavior of $3\text{CaH}_2+4\text{MgB}_2+\text{CaF}_2$ composite was studied by manometric measurements, powder X-ray diffraction, differential scanning calorimetry and attenuated total reflection infrared spectroscopy. The maximum observed quantity of hydrogen loaded in the composite was 7.0 wt%. X-ray diffraction showed the formation of $\text{Ca}(\text{BH}_4)_2$ and MgH_2 after hydrogenation. The activation energy for the dehydrogenation reaction was evaluated by DSC measurements and turns out to be $162 \pm 15 \text{ kJ mol}^{-1} \text{ H}_2$. This value decreases due to cycling to $116 \pm 5 \text{ kJ mol}^{-1} \text{ H}_2$ for the third dehydrogenation step. A decrease of ca. $25^\circ\text{C} - 50^\circ\text{C}$ in dehydrogenation temperature was observed with cycling. Due to its high capacity and reversibility, this composite is a promising candidate as a potential hydrogen storage material.

Keywords: Hydrogen storage, reactive hydride composite, borohydrides, complex hydrides, reaction kinetics, Johnson-Mehl-Avrami.

1. Introduction

Hydrogen storage for stationary as well as mobile applications is a key factor for the development and implementation of hydrogen technologies. Among metal and complex hydrides for hydrogen storage, borohydrides and even more their reactive hydride composites (RHC) i.e. $\text{CaH}_2+\text{MgB}_2+4\text{H}_2 \leftrightarrow \text{Ca}(\text{BH}_4)_2+\text{MgH}_2$ (8.4 wt%) [1-8] offer the potential to meet the requirements for practical applications. To achieve this goal it is necessary to improve the kinetics and tune the thermodynamics of the hydrogenation/dehydrogenation reactions [5, 6, 9]. Orimo et al. [10] demonstrated that by the choice of suitable cation substitution, it is possible to adjust the thermodynamic stabilities of borohydrides. On the other hand, it is also possible to tune

the thermodynamics of the hydrogenation/dehydrogenation reactions in borohydrides by use of the functional anion concept [11]. Hydrogen substitution by fluorine as a dopant or as part of mixed compounds (hydridofluorides) has demonstrated a favorable thermodynamic tailoring for hydrogen storage purposes [12].

The CaF_2 doped composite $3\text{CaH}_2+4\text{MgB}_2+\text{CaF}_2$ has a theoretical hydrogen storage capacity of 7.7 wt% which is similar to that of MgH_2 . However, the dehydrogenation enthalpy in the RHC $\text{Ca}(\text{BH}_4)_2+\text{MgH}_2 \rightarrow \text{CaH}_2+\text{MgB}_2+4\text{H}_2$ is assumed to be much lower, whereby the complexity of the heat management system will be reduced significantly. In contrast to MgH_2 , which shows the dehydrogenation enthalpy of about 65.8 - 75.3 $\text{kJ mol}^{-1} \text{H}_2$ [13], the charged (hydrogenated) $\text{CaH}_2+\text{MgB}_2$ composite, i.e. $\text{Ca}(\text{BH}_4)_2+\text{MgH}_2$, is calculated to have a dehydrogenation enthalpy of 47.0 $\text{kJ mol}^{-1} \text{H}_2$ [13].

In the present work, the hydrogen sorption properties of the $3\text{CaH}_2+4\text{MgB}_2+\text{CaF}_2$ reactive hydride composite are reported. The composite $3\text{CaH}_2+4\text{MgB}_2+\text{CaF}_2$ was intended to produce $\text{Ca}(\text{BH}_4)_2 + \text{MgH}_2$ as main products after hydrogenation and likely Fluorine substituted byproducts i.e. MgF_2 , $\text{Ca}(\text{BF}_4)_2$ or $\text{Ca}(\text{BF}_4\text{H}_{4-x})_2$. By addition of the fluorinated compound CaF_2 , a decrease of the dehydrogenation temperature with respect to the undoped $\text{CaH}_2+\text{MgB}_2$ was observed.

2. Experimental details

A $\text{CaH}_2 / \text{CaF}_2$ mixture was produced in a Spex mill by ball milling for 60 hours. CaH_2 (98% purity, Alfa Aesar) and CaF_2 (99.99% purity, Aldrich) were milled in a molar ratio of 3:1. The molar ratio of the $\text{CaH}_2 / \text{CaF}_2$ mixture was selected with the aim to introduce a significant quantity of F and, simultaneously, to avoid a reduction of the hydrogen storage capacity. As a second step, the $\text{CaH}_2 / \text{CaF}_2$ mixture and MgB_2 (98% purity, Alfa Aesar) were milled together in a Spex mill for 27 hours for a final composition $3\text{CaH}_2+4\text{MgB}_2+\text{CaF}_2$. The sample preparation and milling process were performed in an argon filled glove box. The ball to powder ratio was 10:1 in both stages. Milling was performed in a vial of hardened steel and 10 zirconia balls of 10 mm diameter. For purposes of comparison, a $\text{CaH}_2+\text{MgB}_2$ composite was prepared as described elsewhere [6, 14].

The as-milled composite was heated and exposed to hydrogen atmosphere in a PCTPro-2000 (SETARAM Instrumentation) manometric instrument. Hydrogenation and dehydrogenation experiments were performed at three different temperatures, i.e. 300 °C, 350 °C and 400 °C. The initial hydrogenation pressure was set to 100 bar or 130 bar. An initial pressure of 0.1 bar was fixed for dehydrogenation experiments. In order to collect samples for structural and

thermodynamic characterization, the hydrogenation and dehydrogenation reactions were made in a cumulative way. A sample of the as-milled powder was hydrogenated and then the experiment was stopped. A second sample of the same powder batch was hydrogenated and dehydrogenated, and then the experiment was stopped. A third sample of the same batch was first hydrogenated, dehydrogenated and re-hydrogenated. A fourth sample was exposed to two cycles of hydrogenation/dehydrogenation and so on. Structural changes in each stage of hydrogenation/dehydrogenation were followed by powder X-Ray diffraction (XRD, Bruker AXS, Cu K_{α1}, $\lambda = 1.5406\text{\AA}$). The powders were pressed in a plastic sample holder and sealed with Kapton® foil in order to avoid reaction with moisture. Diffraction patterns were measured in the range from 10-70° in 2 θ , in steps of 0.05° and 12 s per step. All diffractograms were plotted as q [\AA^{-1}] instead of 2 θ degree; with $q = 4\pi\sin(\theta / \lambda)$, where θ is half the scattering angle, and λ is the wavelength.

In order to obtain the temperature dependence behavior and the activation energy of the dehydrogenation reaction, differential scanning calorimetry (DSC) experiments were carried out using a Netzsch STA 409 equipment. The DSC equipment was carefully calibrated by using high purity Pb, In, Sn, Zn and Al wires. Simultaneous DSC and mass spectrometer (MS) analysis were performed (Hiden HPR-20 QIC) to monitor the concentration of H₂ and undesirable reaction byproducts like HF, B₂H₆ and H₂O in the exhaust gas. DSC and MS measurements were performed in an argon filled glove box. The hydrogenated samples were heated from room temperature to 500°C with a heating rate of 2, 5 and 10 °C min⁻¹ under an argon flow of 50 cm³ min⁻¹. The DSC experiments were performed for the first, second and third dehydrogenation segments of hydrogenation/ dehydrogenation cycles. The samples for the DSC measurements were taken after the first, second and third hydrogenation in the PCTPro-2000 manometric instrument. DSC measurements were performed in a nitrogen filled glove box. The IR spectra were recorded on single-reflection ALPHA-Platinum ATR (attenuated total reflection) unit. The spectra were obtained at 2 cm⁻¹ resolution, 64 scans were averaged for each spectrum in the range of 4000-375 cm⁻¹. IR measurements were performed in a nitrogen filled glove box. IR spectra of the as-milled, first hydrogenated, first dehydrogenated and reference compounds, such as Ca(BH₄)₂ and Ca(BF₄)₂ were recorded.

3. Results and discussion

Figure 1 presents hydrogenation measurements of 3CaH₂+4MgB₂+CaF₂ RHC for the first and second hydrogenation, at 130 bar H₂ and 350°C. Under these conditions the amount of stored hydrogen was about 6 - 7 wt% after 12 hours of hydrogenation. In the first hydrogenation a value

of $\alpha=0.8$ (where α is the transformed fraction, i.e. the ratio between the current hydrogen uptake and the final hydrogen uptake) was reached within 4 hours. In the second cycle the value of $\alpha=0.8$ was reached in only 1 hour, indicating a significant improvement of hydrogenation kinetics upon cycling. The inset of Figure 1 presents the analysis of the rate determining step (RDS) of reaction kinetics using one simple model (chemisorption) and four different models for three-dimensional growth, Table I [15, 16]:

a) The surface reaction model (called chemisorption, model equation 1 in Table I) assumes the initial surface reaction of hydrogen molecules on the particle surface being the RDS. b) The Johnson Mehl Avrami (JMA) model, a three dimensional approach, presupposes that nucleation occurs randomly in the bulk and at the surface of the material. Growth is controlled by the interface mobility. In case of pre-existing nuclei, three-dimensional growth and constant interphase velocity, the kinetics would be well described by equation 2 of Table I (called JMA-3D).

c) If the interface migration is decelerating, i.e. diffusion controlled, equation 4 of Table I applies (called JMA-3D DC).

d) If the growth of the new phase starts from the surface to the center of a spherical volume, the contracting-volume three dimensional model is considered. In case of three-dimensional growth with constant interphase velocity, the kinetics ought to be described by equation 5 of Table I (called CV-3D civ).

e) If the rate of product formation decreases proportionally with the thickness of the product barrier layer in a spherical volume, a diffusion-controlled reaction applies. The equation 7 of Table I describes the diffusion controlled with decreasing interface velocity kinetics (CV-3D div). To determine which mechanism rules the reaction, the transformed fraction was substituted in the equations (left side of the model equations) to get the form $f(\alpha)=k \cdot t$. If the model equation, i.e. $f(\alpha)$, presents a linear behavior with time, this model can be assumed as the one that rule the RDS. The quality of the fit is judged by the correlation coefficient R that should be close to 1 [16]. From the slope of the linear fit it is possible to obtain the value of the rate constant. In the present work, the contracting volume three dimensional growth diffusion controlled with decreasing interface velocity model (**CV-3D div**) describes the reaction kinetics best. However two rate constants were obtained at different time periods. The first period is between 0 and 0.5 hour approximately and the second one is above 1 hour to the end of experiment. The rate constant values for the first hydrogenation reaction at 350°C and 130 bar are condensed in Table II. Between 0 and 0.5 hour the reaction is rapid and then a decrease in reaction rate was observed. This suggests a change of the rate limiting step during the hydrogenation. The model then

suggests a fast product film grow up to some critical thickness and then slows. In addition to H atoms diffusion, the diffusion of B atoms between two reacting solids in separate crystal lattices could play an important role in the hydrogenation/ dehydrogenation mechanism of reactive hydride composites. The red lines in the inset of Fig.1 present the calculated behavior of the CV-3D div model with both obtained k . Grey lines indicate the calculated behavior of the other models. Second hydrogenation of the $3\text{CaH}_2+4\text{MgB}_2+\text{CaF}_2$ composite also presents two rate constants (values collected in Table II, plot no shown). The value of the rate constant on the first period indicates an improvement of kinetics with cycling. The second period rate constant does not indicate an improvement with cycling.

Hydrogenation curves obtained at 100 bar / 400°C and 130 bar / 300°C and 350°C for the $3\text{CaH}_2+4\text{MgB}_2+\text{CaF}_2$ composite are presented in Figure 2. The non-fluorinated system $\text{CaH}_2+\text{MgB}_2$ was tested at 100 bar/ 400°C and 130 bar/ 350°C for reference. For the $3\text{CaH}_2+4\text{MgB}_2+\text{CaF}_2$ composite, at 130bar/ 300°C the maximum amount of absorbed hydrogen was about 5.8 wt%; at 130 bar / 350 C was about 7 wt%, and at 100 bar / 400°C the maximum amount of absorbed hydrogen was 4 wt% only. In the non fluorinated system $\text{CaH}_2+\text{MgB}_2$ the maximum quantity of absorbed hydrogen was about 3.5 wt% only. In contrast to the fluorinated system, the final hydrogen uptake in the $\text{CaH}_2+\text{MgB}_2$ composite was less sensitive to the applied temperatures and pressures. Table III summarizes the theoretical and experimental hydrogen storage capacities of the investigated samples. The inset of Figure 2 presents the fit of the contracting-volume three dimensional model with decreasing interface velocity model (**CV-3D div**) for undoped $\text{CaH}_2+\text{MgB}_2$ hydrogenated at 130 bar and 350°C. For comparison, the fit obtained for the $3\text{CaH}_2+4\text{MgB}_2+\text{CaF}_2$ composite was included within the same period. The experimental data of $\text{CaH}_2+\text{MgB}_2$ present clearly two different slopes; values are collected in Table II. Blue lines in the inset of Fig. 2 present the calculated behavior of the CV-3D div model for $\text{CaH}_2+\text{MgB}_2$ composite with both obtained k . The first period rate constant is practically the same as the CaF_2 -doped composite. In the second period the $\text{CaH}_2+\text{MgB}_2$ composite presents a lower rate constant than in the CaF_2 -doped composite. The change in the slope of the composites indicates that the real absorption process is more complicated than the mechanism described by the model. In the non-doped RHC system, and without counting reaction intermediaries and byproducts, we have at least 5 different phases, 4 of them in the solid state and a gaseous one. In addition to particle growth; and as depicted above, we have to consider the mobility and change of chemical environment and bonding of B atoms from MgB_2 to $\text{Ca}(\text{BH}_4)_2$ and viceversa during hydrogenation/ dehydrogenation reactions. The presence of CaF_2 might decrease the direct contact of CaH_2 and MgB_2 slowing down the kinetics, alternatively the intensive mix up of CaF_2 /

CaH₂ could generate lattice defects suitable for the permeation of H and B atoms. Kinetics results suggest the last effect and as result CaF₂ might function as support or seed for the growing of the hydrogenated phase Ca(BH₄)₂.

During dehydrogenation, the possible role of CaF₂ in the reactive hydride composite might be as a dopant that modifies the CaH₂ surroundings. Kim et al [17] suggest the formation of a solid solution of CaF_{2-x}H_x in CaF₂ after doping and cycling Ca(BH₄)₂ with TiF₃ or NbF₅. Kim et al [17] and Rongeat et al [18] claim a possible enhanced reversibility originating from the formation of CaF_{2-x}H_x phases. Lee *et al* suggest that CaF₂ act as seed for the growing of CaH₂ during dehydrogenation of Ca(BH₄)₂+CaF₂ [19]. The structural changes in each stage of milling and hydrogenation / dehydrogenation in 3CaH₂+4MgB₂+CaF₂ reacted at 300°C/ 130 bar and 350°C /130bar were studied by powder X-ray diffraction. Figure 3 shows the X-ray diffraction patterns of as milled CaF₂+3CaH₂. The ball milling of CaF₂+3CaH₂ was intended to produce a solid solution or formation of CaF_{2-x}H_x phases. It was not possible to confirm the formation of CaF_{2-x}H_x phases, whose peak positions are similar to that of CaF₂ [20]. Figure 3 reveals that just a mixture of CaF₂/ CaH₂ was formed. Because of the long milling time (60 hours), a significant peak broadening can be observed, indicating decrease of the particle size. The incorporation of MgB₂ and additional milling time (27 hours) led to further peak broadening compared to the as-milled 3CaH₂+CaF₂ material (Figure 3). In addition, the peak at 3.09 Å⁻¹ matched with iron ((110) ISCD 631734). Iron contamination is produced by debris from the milling vial. Iron is a well known catalyst in hydrogen storage materials [21].

Figure 4 presents the X-ray diffraction patterns collected during two cycles of hydrogenation/dehydrogenation of the 3CaH₂+4MgB₂+CaF₂ composite at 350°C and 130/ 0.1 bar of hydrogen pressure (those corresponding to the results of Figure 1). The formation of Ca(BH₄)₂ + MgH₂ was observed after both hydrogenation cycles. From this figure it is possible to conclude that the reaction conditions are appropriate to form Ca(BH₄)₂ + MgH₂. Undesirable fluorinated byproducts such as MgF₂ were not evident. Fluorine substituted byproducts Ca(BF₄)₂ or Ca(BF₄H_{4-x})₂ were not evident. In addition there are unidentified peaks at 1.60 Å⁻¹ and 2.15 Å⁻¹ in the hydrogenated stages, and at 2.11 Å⁻¹ in the dehydrogenated stages which will be the subject of further studies.

The diffraction patterns of 3CaH₂+4MgB₂+CaF₂ composites cycled at 300°C and 130/ 0.1 bar of hydrogen pressure are presented in Figure 5. Despite the long annealing time (12 hours) the hydrogenation and dehydrogenation reactions were not completed. In addition, in the hydrogenated state Ca₄Mg₃H₁₄ was found as byproduct. The most intense peak of Ca₄Mg₃H₁₄ was signaled in Figure 5; less intense peaks are also present but due to plot stacking some details are

lost. The formation of $\text{Ca}_4\text{Mg}_3\text{H}_{14}$ as side reaction product was proposed by Barkhordarian *et al* [6] in the decomposition of $\text{Ca}(\text{BH}_4)_2 + \text{MgH}_2$ composites. In the same work, further heating led to the decomposition of $\text{Ca}_4\text{Mg}_3\text{H}_{14}$ [6]. In contrast to the hydrogenation at 300°C and 130 bar; no $\text{Ca}_4\text{Mg}_3\text{H}_{14}$ reflections were present in the diffraction patterns of the respective samples hydrogenated at 350°C and 130 bar (Figure 4), indicating its role as an intermediate of the reaction or the occurrence of a different reaction pathway. In Figure 5 there are peaks of unknown phase(s) at 1.59, 2.08, 2.10, 2.11 and 2.24 Å⁻¹ (second dehydrogenation pattern). Further experiments are needed to determine the reaction pathway.

Figure 6 shows the DSC signal obtained during dehydrogenation reactions, measured at 5 °C min⁻¹. The curves, from top to bottom, correspond to the materials: hydrogenated $\text{CaH}_2+\text{MgB}_2$ (ab) as reference and the CaF_2 -doped composite in the first (1abs), second (2abs) and third (3abs) hydrogenated states. In the $\text{CaH}_2+\text{MgB}_2$ (ab) profile, the peak at 149°C corresponds to the α - $\text{Ca}(\text{BH}_4)_2$ to β - $\text{Ca}(\text{BH}_4)_2$ phase transformation [6]. The peaks around 400°C are due to the dehydrogenation reactions. In the plot for $3\text{CaH}_2+4\text{MgB}_2+\text{CaF}_2 - 1\text{ab}$ (first hydrogenation) two endothermic peaks occur below 200°C, one at 147°C and another at 165°C. These peaks are not accompanied by mass loss and therefore can be associated to the α - $\text{Ca}(\text{BH}_4)_2$ to β - $\text{Ca}(\text{BH}_4)_2$ phase transformation. After cycling, the peak at 147 C remained, while the peak at 165°C disappeared. In addition to the decrease in dehydrogenation temperature by adding CaF_2 to $\text{CaH}_2+\text{MgB}_2$, a decrease in the dehydrogenation temperature from the first cycle to the third cycle was observed. The onset and peak dehydrogenation temperatures obtained by DSC are collected in Table IV.

Mass spectrometer measurements corresponding to the first dehydrogenation process are reported in Figure 6. The released gas is hydrogen and it matches with the beginning of the decomposition peak. There is no appreciable release of HF, B_2H_6 or H_2O in the exhaust gas. The second and third dehydrogenation-mass spectrometer profiles (not shown) give the same results, i.e. releasing of H_2 and no other gas.

Figure 7 presents the DSC signal obtained during the third dehydrogenation measured at 2, 5 and 10 °C min⁻¹. Similar experiments were carried out for the first and second dehydrogenation. Activation energies were determined from the DSC data using the Kissinger method [22, 23]. The variation of dehydrogenation peak temperatures with heating rate can be used to estimate the apparent activation energy according to:

$$\ln\left(\frac{\beta}{T^2}\right) = -\frac{E_a}{RT} + \ln\left(\frac{AR}{E}\right) + \ln\phi, \quad (8)$$

where E_a is the activation energy, β is the heating rate, T is the peak temperature in K, A is the pre-exponential factor, R the universal gas constant and ϕ is an appropriate function of α [23].

The activation energy is taken from the slope of a plot of the left side of equation (8) versus the inverse of temperature. The activation energy estimated for the first dehydrogenation reaction was $162 \pm 15 \text{ kJ mol}^{-1}$, whereas the value for the third dehydrogenation was $116 \pm 5 \text{ kJ mol}^{-1}$ (inset of Figure 7, Table IV). There is a reduction in the dehydrogenation activation energy with cycling. In order to compare the activation energy values and avoid the presence of hydrogenation byproducts, a sample of freshly ball milled [6] $\text{Ca}(\text{BH}_4)_2 + \text{MgH}_2$ was tested by DSC in the same conditions. The dehydrogenation apparent activation energy for $\text{Ca}(\text{BH}_4)_2 + \text{MgH}_2$ was $169 \pm 15 \text{ kJ mol}^{-1}$. These values indicate a rather small effect of CaF_2 doping in dehydrogenation activation energy, but enough to observe a significant decrease of ca. $25^\circ\text{C} - 50^\circ\text{C}$ (Fig. 6) in dehydrogenation temperature.

The studied samples were additionally characterized with IR-ATR spectroscopy. The spectra of the as-milled, first hydrogenated at 130bar / 350°C and first dehydrogenated $3\text{CaH}_2 + 4\text{MgB}_2 + \text{CaF}_2$ are presented together with the reference spectra of $\text{Ca}(\text{BH}_4)_2$ and $\text{Ca}(\text{BF}_4)_2$ in Figure 8. In the spectra of the first hydrogenated composite the IR manifestations of $\text{Ca}(\text{BH}_4)_2$ are clearly visible. They include the peaks in the $2550\text{-}2100 \text{ cm}^{-1}$ region, which are due to the stretching of B-H bonds of BH_4^- tetrahedra, and the bending modes of HBH in the $1350\text{-}1050 \text{ cm}^{-1}$ region [24]. The presence of these IR features clearly confirms the formation of $\text{Ca}(\text{BH}_4)_2$ after first hydrogenation of the $3\text{CaH}_2 + 4\text{MgB}_2 + \text{CaF}_2$ RHC. A small shift in peak positions between the reference $\text{Ca}(\text{BH}_4)_2$ and the hydrogenated sample of approximately 6 cm^{-1} was also observed. This shift can indicate change in the surroundings of $[\text{BH}_4]^-$ compared to that of pure $\text{Ca}(\text{BH}_4)_2$. In the as-milled sample and after dehydrogenation, the $\text{Ca}(\text{BH}_4)_2$ features are missing or have low intensity, confirming the reversibility of the $3\text{CaH}_2 + 4\text{MgB}_2 + \text{CaF}_2$ RHC.

$\text{Ca}(\text{BF}_4)_2$ was included in order to test for possible fluorine substitution in the RHC during cycling. The main stretching and bending features of $\text{Ca}(\text{BF}_4)_2$ include a broad intense peak at ca. 940 cm^{-1} , which corresponds to B-F stretching; peaks at ca. 500 cm^{-1} that correspond to bending modes of FBF; and a broad unidentified peak in the $1300\text{-}1700 \text{ cm}^{-1}$ region. The noise base line of the composites in the region $1000 - 500 \text{ cm}^{-1}$ makes difficult the identification and assignment of the peaks of B-F and FBF if any, especially in the 940 cm^{-1} region. So, from these experiments, no evidences F substitution was found.

4. Conclusions

$3\text{CaH}_2 + 4\text{MgB}_2 + \text{CaF}_2$ composite is a new hydrogen storage material which can absorb up to 7 wt% of hydrogen. Fluorine addition can be regarded as being beneficial in the frame of reactive hydride composites. A significant increase in the experimental hydrogen uptake capacity in the

$3\text{CaH}_2+4\text{MgB}_2+\text{CaF}_2$ composite compared to pure $\text{CaH}_2+\text{MgB}_2$ composite tested under the same conditions was observed. By means of ex situ-XRD it was possible to confirm the products of hydrogenation as $\text{Ca}(\text{BH}_4)_2$, MgH_2 and $\text{Ca}_4\text{Mg}_3\text{H}_{14}$ as byproduct. Dehydrogenation products were CaH_2 , MgB_2 , 4H_2 and Mg . CaF_2 can be considered as a dopant affecting the hydrogenation kinetics. There is a reduction in the dehydrogenation apparent activation energy by CaF_2 doping and as cycling proceeds; this is related directly with the reduction in the dehydrogenation temperature of ca $25^\circ\text{C} - 50^\circ\text{C}$.

5. References.

- [1] M. Dornheim, N. Eigen, G. Barkhordarian, T. Klassen, R. Bormann, *Advanced Engineering Materials* 8 (2006) 377-385.
- [2] E. Deprez, A. Justo, T.C. Rojas, C. Lopez-Cartes, C. Bonatto Minella, U. Boesenberg, M. Dornheim, R. Bormann, A. Fernandez, *Acta Materialia* 58 (2010) 5683-5694.
- [3] S. Orimo, Y. Nakamori, J.R. Eliseo, A. Zuttel, C.M. Jensen, *Chem. Rev.* 107 (2007) 4111-4132.
- [4] S.V. Alapati, J.K. Johnson, D.S. Sholl, *J. Phys. Chem. B* 110 (2006) 8769-8776.
- [5] S.V. Alapati, J.K. Johnson, D.S. Sholl, *J. Phys. Chem. C* 111 (2007) 1584-1591.
- [6] G. Barkhordarian, T.R. Jensen, S. Doppiu, U. Boesenberg, A. Borgschulte, R. Gremaud, Y. Cerenius, M. Dornheim, T. Klassen, R. Bormann, *J. Phys. Chem. C* 112 (2008) 2743-2749.
- [7] U. Boesenberg, S. Doppiu, L. Mosegaard, A. Borgschulte, N. Eigen, G. Barkhordarian, T. Jensen, O. Gutfleisch, T. Klassen, M. Dornheim, R. Bormann, *Acta Materialia* 55 (2007) 3951 – 3958.
- [8] J.J. Vajo, G.L. Olson, *Viewpoint Set. Scripta Materialia* 56 (2007) 829-834.
- [9] M. Dornheim, S. Doppiu, G. Barkhordarian, U. Boesenberg, T. Klassen, O. Gutfleisch, R. Bormann, *Viewpoint Set in Scripta Materialia* 56 (2007) 841-846.
- [10] H.W. Lee, S. Orimo, Y. Nakamori, K. Miwa, N. Ohba, S. Towata, A. Zuttel, *J. Alloys and Compounds* 446-447 (2007) 315-318.
- [11] H.W. Brinks, A. Fossdal, B.C. Hauback, *J. Phys. Chem. C* 112 (2008) 5658-5661.
- [12] N. Eigen, U. Boesenberg, J Bellosta von Colbe, T.R. Jensen, Y. Cerenius, M. Dornheim, T. Klassen, R. Bormann, *J. Alloys and Compounds*, 477 (2009) 76-80.
- [13] D.J. Siegel, C. Wolverton, V. Ozolins, *Physical review B* 76 (2007) 134102-1 134102-6.
- [14] G. Barkhordarian, T. Klassen, M. Dornheim, R. Bormann, *J. Alloys and Compounds* 400 (2007) L18-L21.
- [15] G. Barkhordarian, T. Klassen, R. Bormann, *J. Alloys and Compounds* 407 (2006) 249-255.

- [16] U. Boesenberg, J.W. Kim, D. Gossler, N. Eigen, T.R. Jensen, J.M. Bellosta von Colbe, Y. Zhou, M. Dahms, D.H. Kim, R. Gunther, Y.W. Cho, K.H. Oh, T. Klassen, R. Bormann, M. Dornheim, *Acta Materialia* 58 (2010) 3381-3389.
- [17] J.H. Kim, J.H. Shim, Y.W. Cho, *J. Power Sources* 181 (2008) 140-143.
- [18] C. Rongeat, V. D'Anna, H. Hagemann, A. Borgschulte, A. Zuttel, L. Schultz, O. Gutfleisch, *J. Alloys and Compounds* 493 (2010) 281- 287.
- [19] J.Y. Lee, Y.S. Lee, J.Y. Suh, J.H. Shim, Y. Whan Cho, *J. of Alloys and Compounds* 506 (2010) 721-727.
- [20] J.F. Brice, A. Courtois, J. Aubry, *J. Sol. State Chem.* 24 (1978) 381- 387.
- [21] B. Sakintunaa, F. Lamari-Darkrim, M. Hirscher, *International Journal of Hydrogen Energy* 32 (2007) 1121 – 1140.
- [22] H.E. Kissinger, *Anal. Chem.* 29 (1957) 1702- 1706.
- [23] J.P. Elder, *J. Thermal Analysis* 30 (1985) 657-669.
- [24] M. Fichtner, K. Chlopek, M. Longhini, H. Hagemann, *J. Phys. Chem. C* 112 (2008) 11575–11579.

6. Acknowledgments

The authors appreciate the financial support from the European Union in the frame of the collaborative project “FLYHY - Fluorine Substituted High Capacity Hydrides for Hydrogen Storage at low Working Temperatures” (Grant agreement no.: N° 226943).

Table I: Equations and description of the kinetic models [15, 16].

	Model equation	Description
1	$\alpha = kt$	Surface controlled (chemisorption) [15]
2	$[-\ln(1-\alpha)]^{1/3} = kt$	JMA 3D growth of existing nuclei with constant interface velocity [15]
3	$[-\ln(1-\alpha)]^{1/2} = kt$	JMA: 2D growth of existing nuclei with constant interface velocity [15]
4	$[-\ln(1-\alpha)]^{2/3} = kt$	JMA-3D-DC : Three-dimensional growth of random nuclei with decreasing interface velocity, diffusion controlled [16]
5	$1-[1-\alpha]^{1/3} = kt$	CV-3D civ : contracting volume, 3D growth with constant interface velocity [15, 16]
6	$1-[1-\alpha]^{1/2} = kt$	CV: contracting volume, 2D growth with constant interface velocity [15]
7	$1-\frac{2\alpha}{3}-(1-\alpha)^{2/3} = kt$	CV-3D div : contracting volume, 3D growth diffusion controlled with decreasing interface velocity [15]

Table II. Hydrogenation rate constant for the contracting volume three dimensional growth diffusion-controlled with decreasing interface velocity model (CV-3D div)

Material and condition	0 ~ 0.5 hour k [s ⁻¹]	1-10 hour period k [s ⁻¹]
3CaH ₂ + 4MgB ₂ + CaF ₂ First absorption 350°C / 130bar	1.83 x 10 ⁻⁵	5.33 x 10 ⁻⁶
3CaH ₂ + 4MgB ₂ + CaF ₂ Second absorption 350°C / 130bar	3.71 x 10 ⁻⁵	2.82 x 10 ⁻⁶
CaH ₂ + MgB ₂ First absorption 350°C / 130bar	1.85 x 10 ⁻⁵	3.89 x 10 ⁻⁶

Table III. Theoretical and experimental hydrogen uptake capacity (first hydrogenation)

Composite and conditions	Theoretical H ₂ capacity [wt.%]	Experimental H ₂ capacity [wt.%]
CaH ₂ + MgB ₂ 400°C / 100 bar	8.3	3.3
CaH ₂ + MgB ₂ 350°C / 130 bar	8.3	3.5
3CaH ₂ + 4MgB ₂ + CaF ₂ 300°C / 130bar	7.7	5.8
3CaH ₂ + 4MgB ₂ + CaF ₂ 350°C / 130bar	7.7	7.0
3CaH ₂ + 4MgB ₂ + CaF ₂ 400°C / 100bar	7.7	4.0

Table IV. Dehydrogenation temperatures and activation energy for $3\text{CaH}_2+4\text{MgB}_2+\text{CaF}_2$ composites

Heating rate	1 st dehydrogenation		2 nd dehydrogenation		3 rd dehydrogenation	
	Onset T	Peak T	Onset T	Peak T	Onset T	Peak T
2 K min ⁻¹	299 °C	367 °C	263 °C	300 °C	255 °C	291 °C
5 K min ⁻¹	321 °C	388 °C	277 °C	319 °C	275 °C	312 °C
10 K min ⁻¹	329 °C	401 °C	294 °C	333 °C	281 °C	327 °C
Activation energy	162 ± 15 kJ mol ⁻¹ H ₂		132 ± 5 kJ mol ⁻¹ H ₂		116 ± 5 kJ mol ⁻¹ H ₂	

Figure caption

Fig. 1 – First and second hydrogenation measurement of $3\text{CaH}_2+4\text{MgB}_2+\text{CaF}_2$ composite at 350°C and 130bar. Inset: application of kinetics model formulae to first hydrogenation.

Fig.2 – First hydrogenation measurement of $3\text{CaH}_2+4\text{MgB}_2+\text{CaF}_2$ and $\text{CaH}_2+\text{MgB}_2$ composites at different conditions of temperature and hydrogen pressure. Inset: contracting-volume three dimensional model for $3\text{CaH}_2+4\text{MgB}_2+\text{CaF}_2$ and $\text{CaH}_2+\text{MgB}_2$ composites at 130bar and 350°C .

Fig. 3 – XRD patterns of $\text{CaF}_2+3\text{CaH}_2$ (below) and $3\text{CaH}_2+4\text{MgB}_2+\text{CaF}_2$ (above) as-milled materials.

Fig. 4 – XRD patterns of $3\text{CaH}_2+4\text{MgB}_2+\text{CaF}_2$ composite, after hydrogenation and dehydrogenation at 350°C and 130bar or 0.1bar respectively.

Fig. 5 - XRD patterns of $3\text{CaH}_2+4\text{MgB}_2+\text{CaF}_2$ composite, after hydrogenation and dehydrogenation at 300°C and 130bar or 0.1bar respectively.

Fig. 6 - DSC signal, dehydrogenation of first hydrogenated $\text{CaH}_2+\text{MgB}_2$; first, second and third hydrogenated $3\text{CaH}_2+4\text{MgB}_2+\text{CaF}_2$ at 5°C min^{-1} (left). Mass spectrometer signal of first hydrogenated $3\text{CaH}_2+4\text{MgB}_2+\text{CaF}_2$ (right).

Fig. 7 - DSC measurements for third dehydrogenation reaction (2°C min^{-1} , 5°C min^{-1} , $10^\circ\text{C min}^{-1}$) and activation energy plot.

Fig. 8 - ATR-IR spectra of as-milled, hydrogenated (1ab) and dehydrogenated (1de) $3\text{CaH}_2+4\text{MgB}_2+\text{CaF}_2$. The spectra of $\text{Ca}(\text{BH}_4)_2$ and $\text{Ca}(\text{BF}_4)_2$, are shown for comparison. The noise at *ca.* $2000\text{-}2100\text{ cm}^{-1}$ corresponds to low transmittance of diamond ATR crystal in this region.

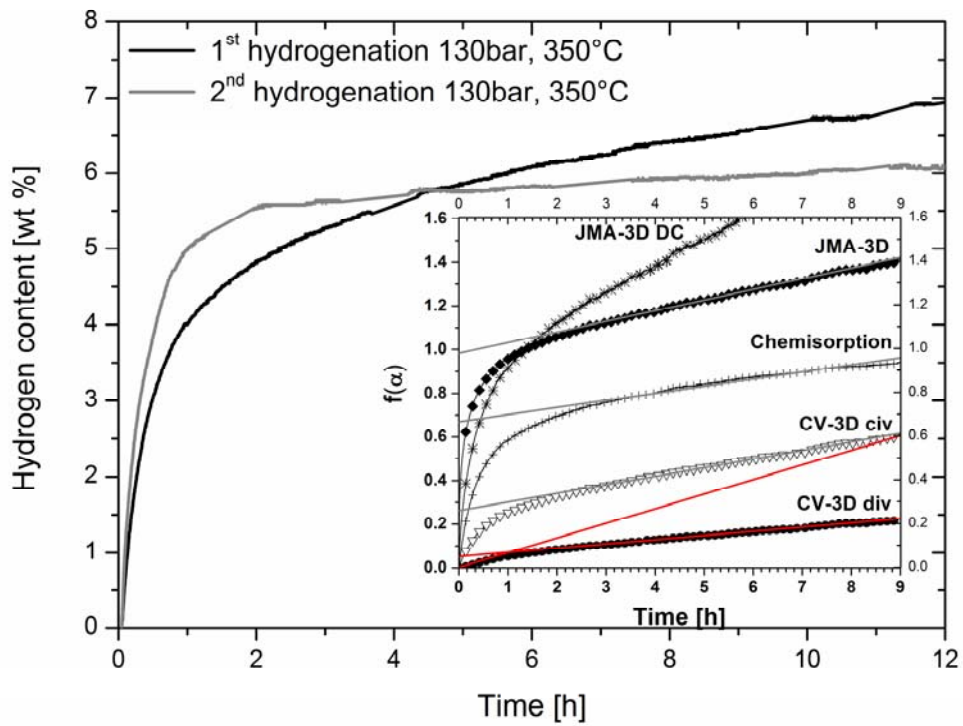


Fig. 1 – First and second hydrogenation measurement of $3\text{CaH}_2+4\text{MgB}_2+\text{CaF}_2$ composite at 350°C and 130bar . Inset: application of kinetics model formulae to first hydrogenation.

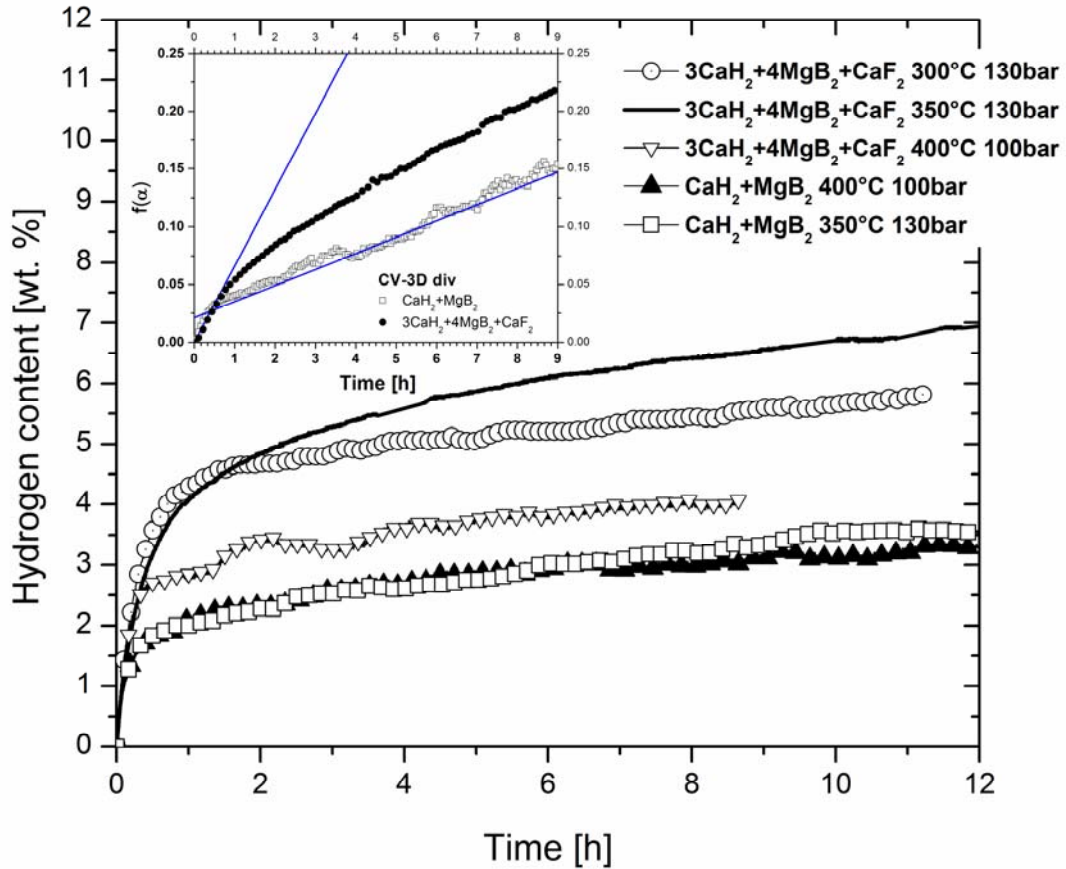


Fig.2 – First hydrogenation measurement of $3\text{CaH}_2+4\text{MgB}_2+\text{CaF}_2$ and $\text{CaH}_2+\text{MgB}_2$ composites at different conditions of temperature and hydrogen pressure. Inset: contracting-volume three dimensional model for $3\text{CaH}_2+4\text{MgB}_2+\text{CaF}_2$ and $\text{CaH}_2+\text{MgB}_2$ composites at 130bar and 350°C.

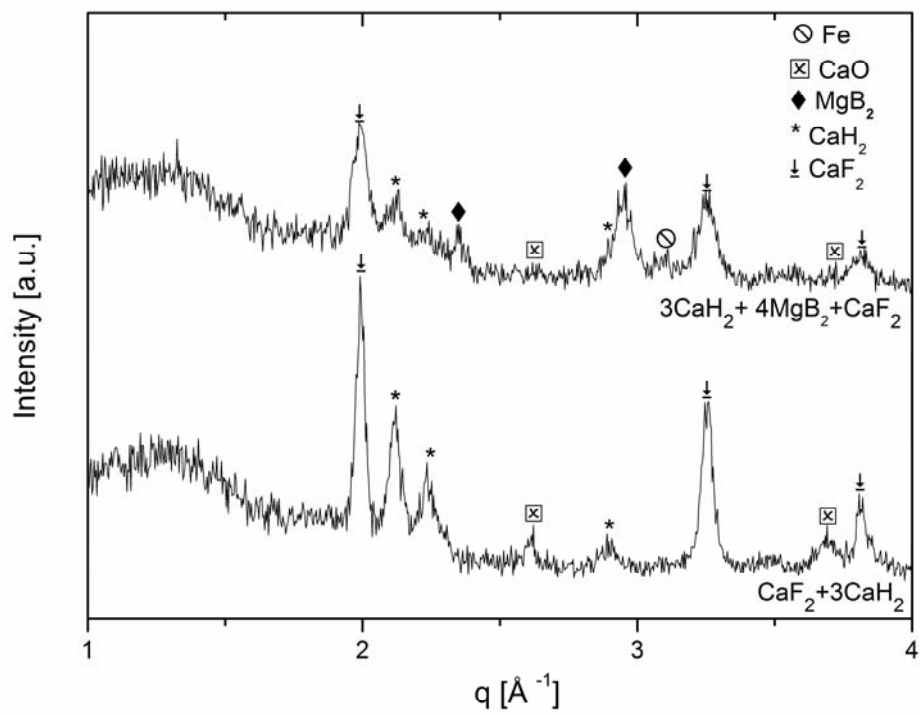


Fig. 3 – XRD patterns of CaF₂+3CaH₂ (below) and 3CaH₂+4MgB₂+CaF₂ (above) as-milled materials.

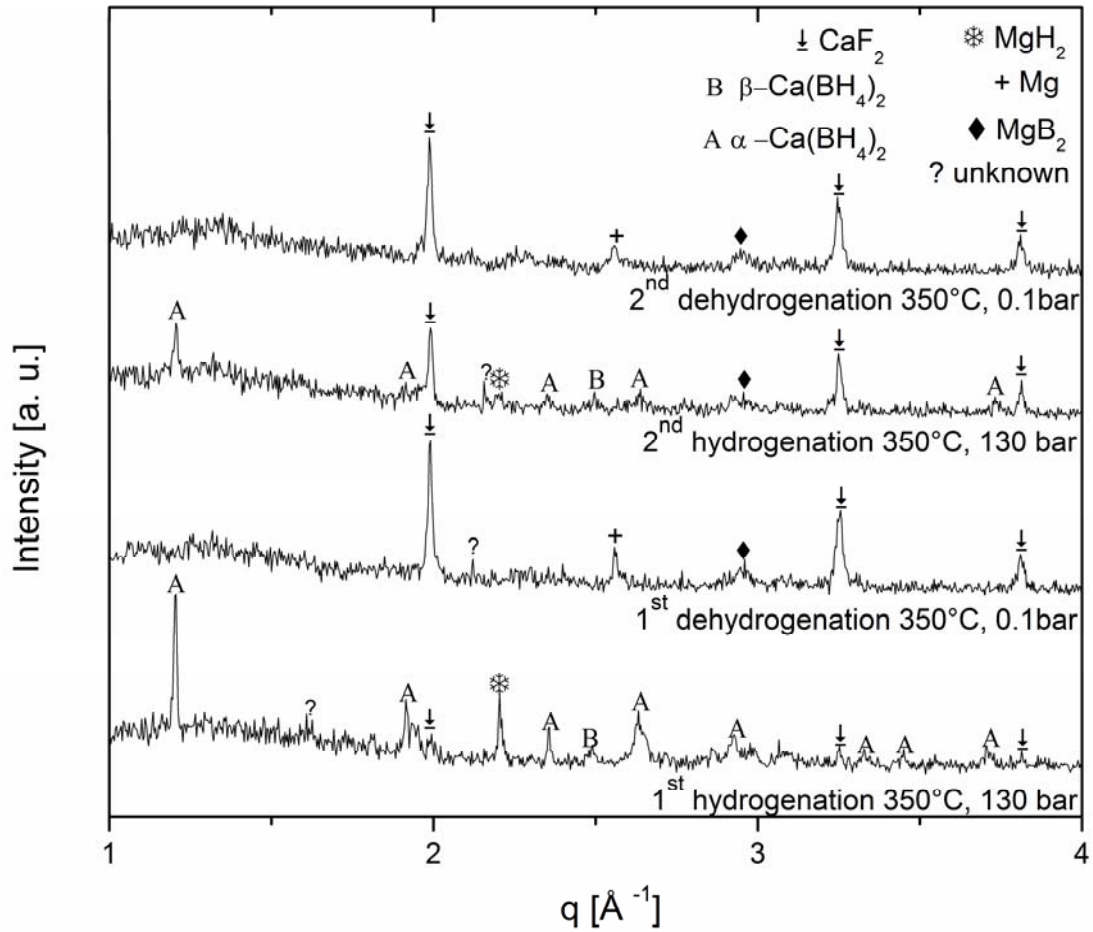


Fig. 4 – XRD patterns of $3\text{CaH}_2+4\text{MgB}_2+\text{CaF}_2$ composite, after hydrogenation and dehydrogenation at 350°C and 130bar or 0.1bar respectively.

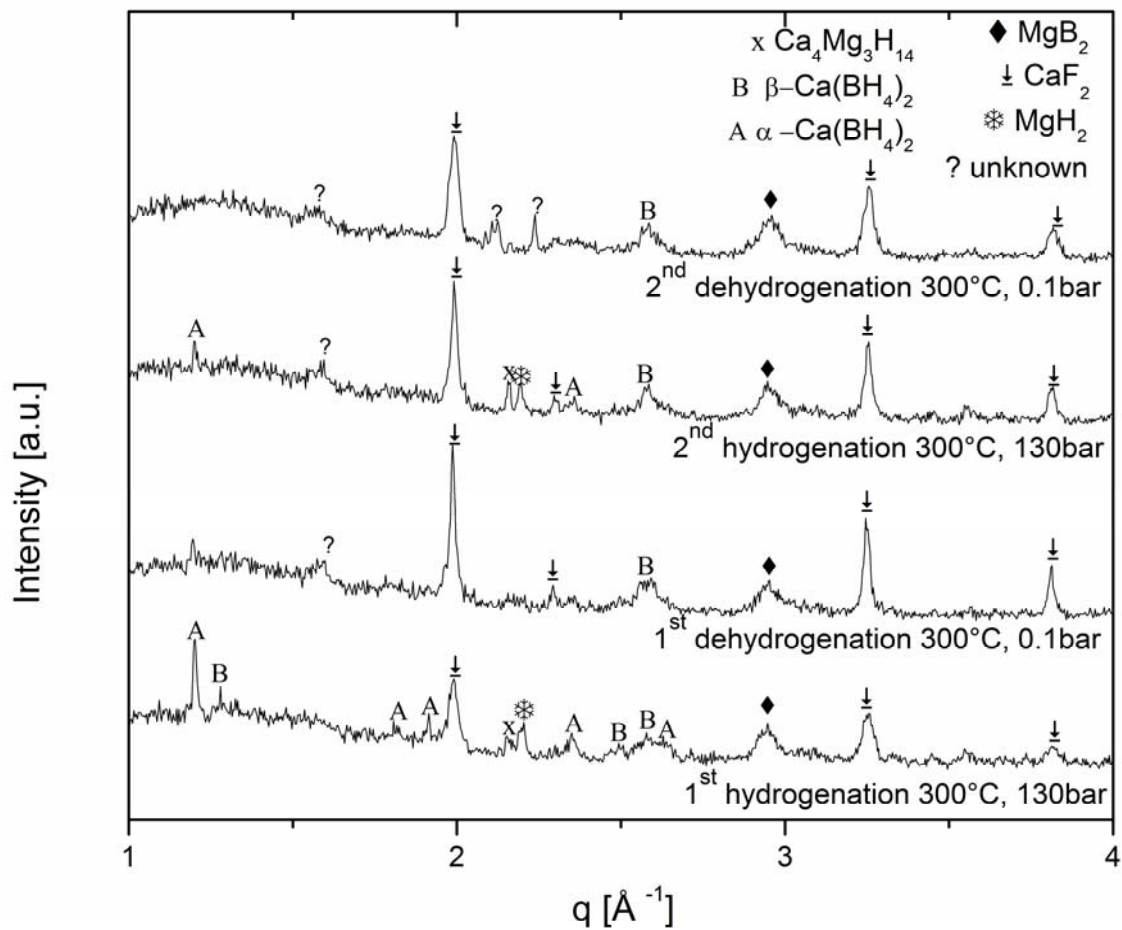


Fig. 5 - XRD patterns of $3\text{CaH}_2+4\text{MgB}_2+\text{CaF}_2$ composite, after hydrogenation and dehydrogenation at 300°C and 130bar or 0.1bar respectively.

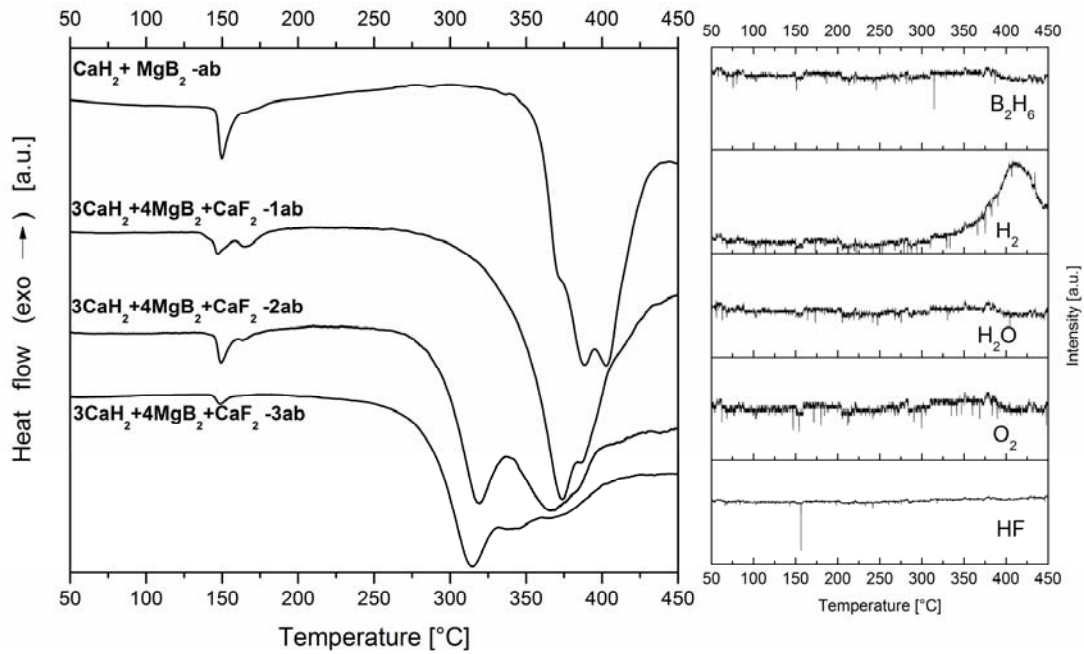


Fig. 6 - DSC signal, dehydrogenation of first hydrogenated $\text{CaH}_2 + \text{MgB}_2$; first, second and third hydrogenated $3\text{CaH}_2 + 4\text{MgB}_2 + \text{CaF}_2$ at 5 °C min^{-1} (left). Mass spectrometer signal of first hydrogenated $3\text{CaH}_2 + 4\text{MgB}_2 + \text{CaF}_2$ (right).

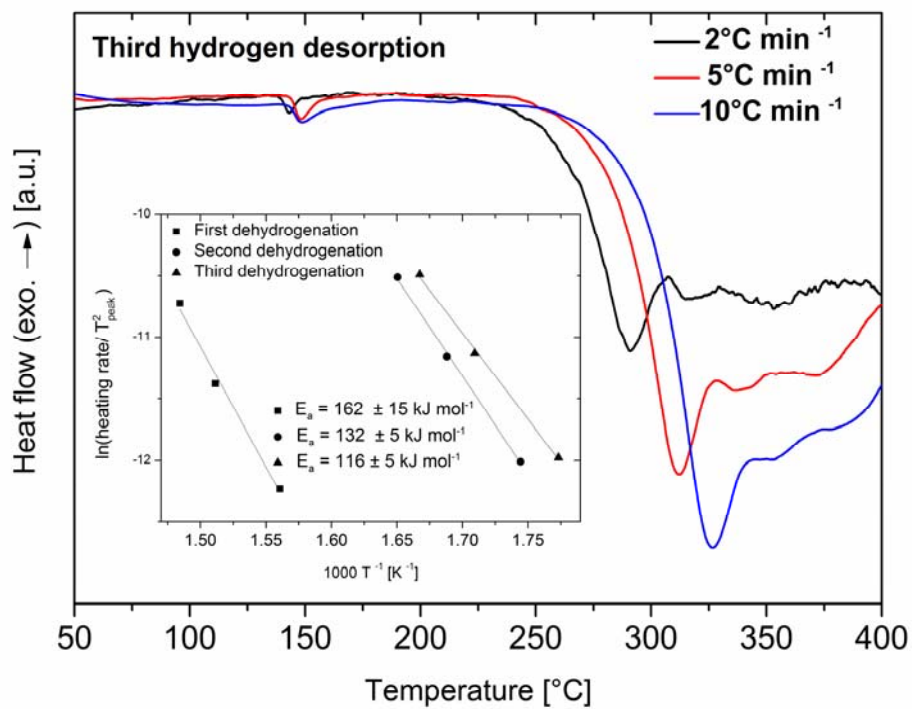


Fig. 7 - DSC measurements for third dehydrogenation reaction (2 °C min⁻¹, 5 °C min⁻¹, 10 °C min⁻¹) and activation energy plot.

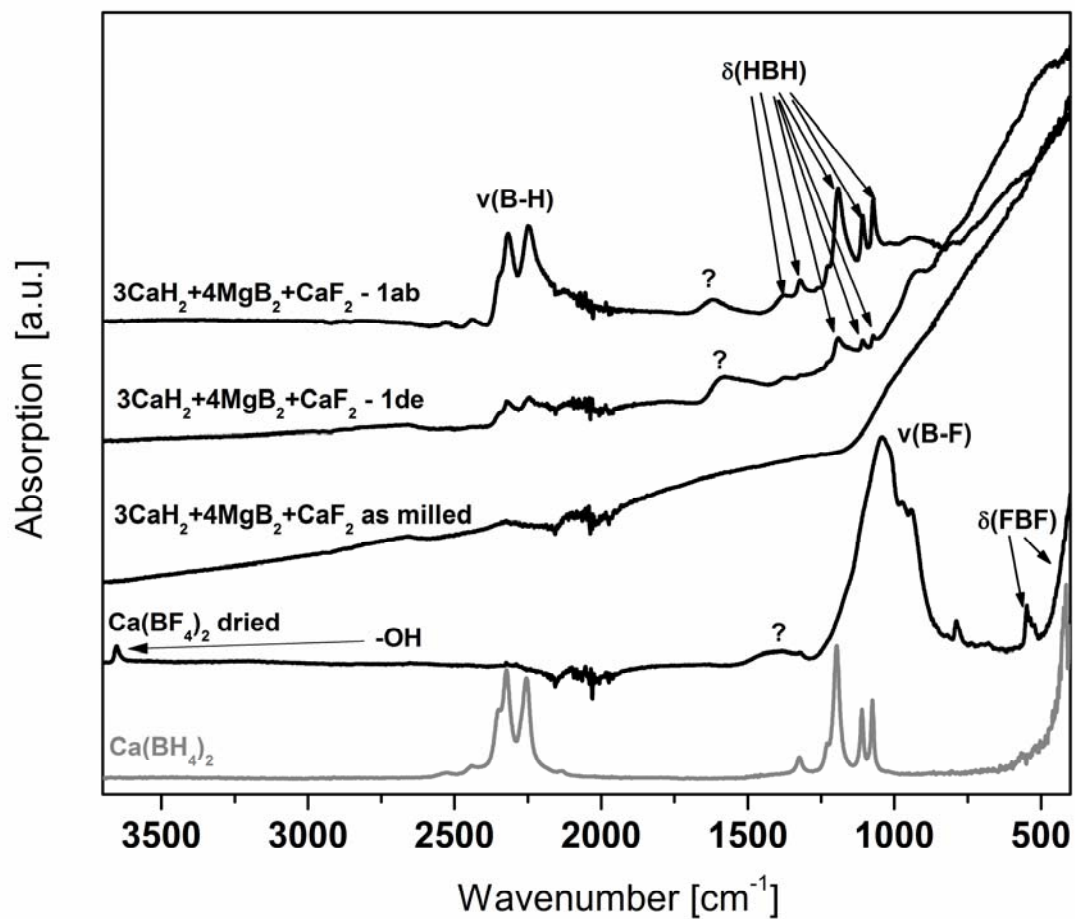


Fig. 8 - ATR-IR spectra of as-milled, hydrogenated (1ab) and dehydrogenated (1de) $3\text{CaH}_2+4\text{MgB}_2+\text{CaF}_2$. The spectra of $\text{Ca}(\text{BH}_4)_2$ and $\text{Ca}(\text{BF}_4)_2$, are shown for comparison. The noise at *ca.* 2000-2100 cm^{-1} corresponds to low transmittance of diamond ATR crystal in this region.